ACCOUNTS
of chemical research

Recent Advances in the Application of Electron Tomography to Materials Chemistry

ROWAN LEARY,* PAUL A. MIDGLEY,* AND
JOHN MEURIG THOMAS*

Department of Materials Science and Metallurgy, University of Cambridge, Pembroke Street, Cambridge CB2 3QZ, United Kingdom.

RECEIVED ON APRIL 16, 2012

CONSPECTUS

Nowadays, tomography plays a central role in pureand applied science, in medicine, and in many branches of engineering and technology. It entails reconstructing the three-dimensional (3D) structure of an object from a tilt series of two-dimensional (2D) images. Its origin goes back to 1917, when Radon showed mathematically how a series of 2D projection images could be converted to the 3D structural one. Tomographic X-ray and positron scanning for 3D medical imaging, with a resolution of ∼1 mm, is now ubiquitous in major hospitals. Electron tomography, a relatively new chemical tool, with a resolution of ∼1 nm, has been recently adopted by materials chemists as an invaluable aid for the 3D study of the morphologies, spatially-discriminating chemical compositions, and defect properties of nanostructured materials.

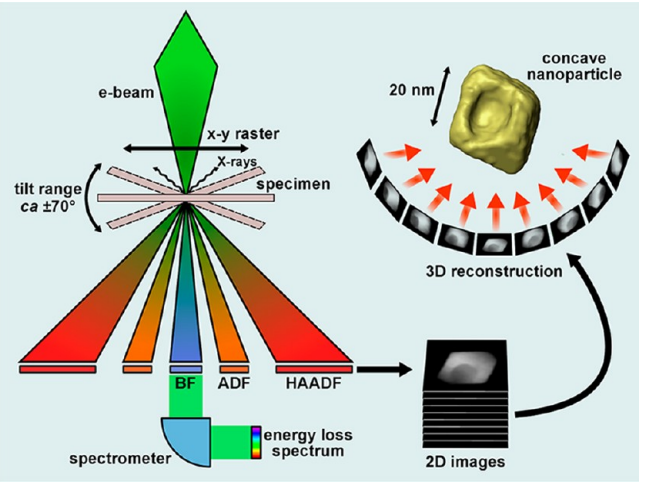

In this Account, we review the advances that have been made in facilitating the recording of the required series of 2D electron microscopic images and the subsequent process of 3D reconstruction of specimens that are vulnerable, to a greater or lesser degree, to electron beam damage. We describe how high-fidelity 3D tomograms may be obtained from relatively few 2D images by incorporating prior structural knowledge into the reconstruction process. In particular, we highlight the vital role of compressed sensing, a recently developed procedure well-known to information theorists that exploits ideas of image compression and "sparsity" (that the important image information can be captured in a reduced data set). We also touch upon another promising approach, "discrete" tomography, which builds into the reconstruction process a prior assumption that the object can be described in discrete terms, such as the number of constituent materials and their expected densities. Other advances made recently that we outline, such as the availability of aberration-corrected electron microscopes, electron wavelength monochromators, and sophisticated specimen goniometers, have all contributed significantly to the further development of quantitative 3D studies of nanostructured materials, including nanoparticle-heterogeneous catalysts, fuel-cell components, and drug-delivery systems, as well as photovoltaic and plasmonic devices, and are likely to enhance our knowledge of many other facets of materials chemistry, such as organic−inorganic composites, solar-energy devices, bionanotechnology, biomineralization, and energy-storage systems composed of high-permittivity metal oxides.

1. Introduction

More than a decade has elapsed since two of us[1] began to exploit atomic number (*Z*)−contrast electron microscopy in a three-dimensional (3D) mode for the recovery of unique kinds of information pertaining to the shape, composition, and other significant features of high-performance bimetallic nanocluster and nanoparticle heterogeneous catalysts.[2] In the intervening time, several reviews of electron tomography (ET) of relevance to nanochemical research have appeared.[3,4] ET, and in particular the technique of ET using high-angle annular dark-field scanning transmission electron microscopy (HAADF-STEM, see Figure 1), which we have

Published on the Web 08/17/2012 www.pubs.acs.org/accounts
10.1021/ar3001102

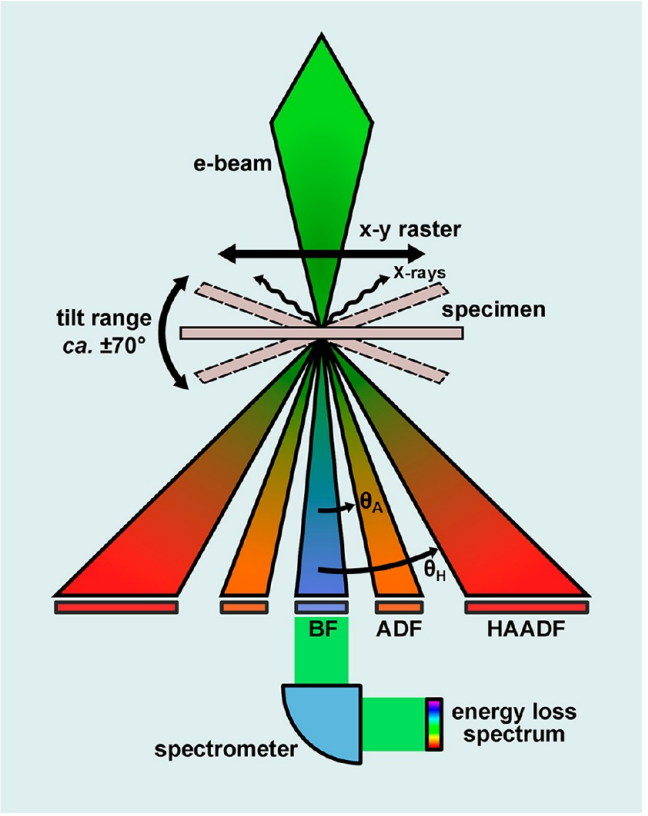

FIGURE 1. The STEM and associated detectors: high-angle annular dark-field (HAADF), annular dark-field (ADF), and bright-field (BF). If the BF detector is removed, transmitted electrons can pass through a spectrometer to form an energy-loss spectrum. The tilting of the specimen performed in ET experiments is illustrated schematically. $\theta_A \approx 10$ mrad and $\theta_H \approx 50$ mrad.

exclusively favored,[5,6] has recently progressed in a remarkably significant manner for several reasons. First, it has now reached a quantitative status. Second, the greatly improved spatial resolution made possible by aberration-corrected (AC) microscopes (<0.5 Å) has opened up several new avenues of enquiry. Third, modern hardware, such as computer-controlled goniometers (that can more rapidly and accurately achieve angular settings for recording the 2D images), novel tomography holders, and much improved electron detectors are now readily available. Fourth, there have been major developments in new imaging modes to elucidate not merely morphology but also composition, electronic status, and other physicochemical parameters in 3D. Finally, these advances in acquisition have been complemented by the development of new algorithms for image reconstruction and visualization in robust and reliable forms. In particular, the so-called procedures of discrete tomography (DT)[7] and compressed sensing (CS)[8,9] can be invoked in ET to yield high-fidelity reconstructions from only a small number of images, a capability of significance for studying electron-beam sensitive samples like biological macromolecules and biominerals. As we outline below, with a greater focus on CS-ET methods with which our group has primarily been concerned, these approaches provide further advantages in the retrieval, via ET, of tomographic information both in 3D and in the recently introduced technique of 4D electron microscopy,[10,11] whereby it becomes possible simultaneously to record picometer spatial and femtosecond time precisions.

2. STEM and ET

One of the key microscopic modes available to the materials chemist is STEM, the great benefit of which is that with a single incident probe of sub-nanometer (and sometimes sub-Ångström) diameter, it is possible to detect many signals emanating from a minute volume of material, as little as a zeptogram (10^{-21} g), for example,[12] each of which leads to an image endowing complementary information about the sample. These include bright-field (BF), annular dark-field (ADF) and high-angle annular dark-field (HAADF) signals. For each signal, a separate detector is used to capture different angular ranges of the scattered beam (Figure 1). In addition to these structural imaging modes, it is possible simultaneously to record a variety of spectroscopic signals such as electron energy-loss (EEL) and X-ray emission spectra. The use of AC-optics for STEM imaging and microanalysis allows all this to occur at near atomic resolution: one can identify the chemical elements present and, in favorable circumstances, their electronic configurations.

STEM yields 2D images of a 3D object, and in many cases, these may be considered to represent a "projection" of some physical quantity of the 3D object.[4,6] ET is achieved by recording a series of 2D images at various angles, usually about a single axis (perpendicular to the plane of the diagram in Figure 1, see Figure 2a). Typically, tilt increments of 1−2° are used, over an angular range of ca. ±70°; the limited space between the pole pieces of the microscope objective lens often prevents rotation over a complete ±90°. The ensemble of images is then used to form a 3D reconstruction or *tomogram*, usually via a "back-projection" process (Figure 2b).[13] The smaller the angular increment and the greater the angular range, the higher the resolution of the tomogram.[14]

3. ET in Nanoscale Materials Chemistry

3.1. HAADF-STEM Tomography of Supported Heterogeneous Catalysts. Although its use across the field of materials chemistry is wide-ranging, perhaps the greatest

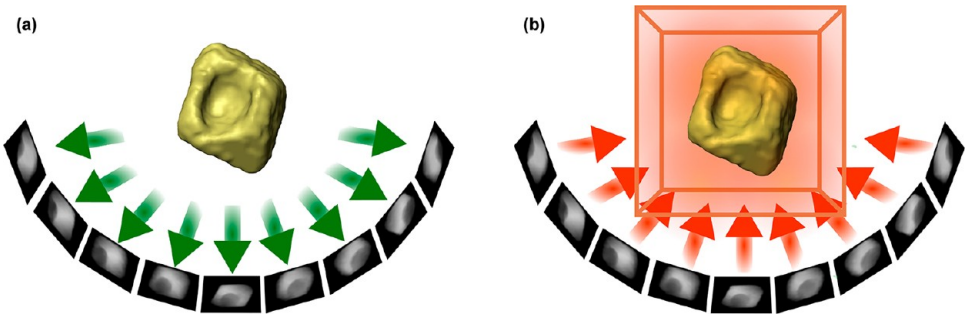

FIGURE 2. Schematic representation of (a) the acquisition of a "tilt series" of 2D images of an object (in this case a concave iron oxide nanoparticle) and (b) back-projection of these images into a 3D space to obtain a reconstruction of the object.

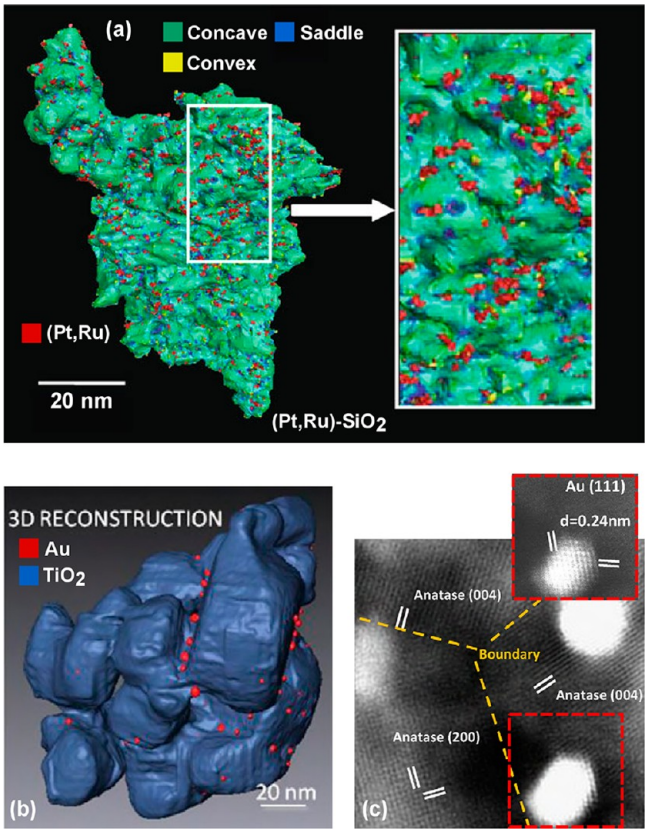

FIGURE 3. (a) ET reconstruction of (Pt,Ru) nanocatalysts supported on a disordered mesoporous silica. The surface-rendered visualization of the silica support has been color-coded according to the local Gaussian curvature. The nanocatalysts (red) appear to prefer to anchor themselves at the (blue) saddle-points.[15] (b) Surface-rendered visualization of an ET reconstruction of Au nanocatalysts (red) supported on titania (blue). The nanocatalysts are located in the crevices between titania crystallites; confirmed by the AC-STEM image in panel (c).[16]

impact of ET to date has been in the study of supported metallic nanocluster catalysts. We first draw upon our own work, highlighting a study[15] of bimetallic (Pt,Ru) nanocluster catalysts supported on mesoporous silica, where such nanocatalysts may be almost invisible using conventional BF-TEM yet can be readily distinguished from the lighter support material using HAADF-STEM imaging, owing to the strong *Z*-dependence of the HAADF signal.[6] From the ET reconstruction, the pore volume, surface area, mean diameter, overall porosity, and catalyst loading were determined, and the surface dimension of the pore network was found to be fractal in nature. Moreover, by classifying the surface curvature of the support, the nanocatalysts were found to prefer to be anchored at "saddle-points" on the support surface (Figure 3a). In another example[16] (Figure 3b,c), a combination of AC-(S)TEM and HAADF-STEM tomography identified that Au nanocatalysts on titania show a propensity to reside in crevices between the individual titania grains.

In a recent study[17] of (Pt,Co) nanocatalysts on a fuel cell carbon support, electrochemical experiments were undertaken using the TEM sample support grid as the working electrode in a three electrode cell. STEM-based tomographic reconstructions, made before and after electrochemical aging, revealed changes to the 3D morphologies and locations of the nanocluster electrocatalysts that when combined with STEM–EEL spectroscopy enabled determination of the primary cause of particle coarsening.

3.2. 3D Analysis of Nanoporous Solids. Although traditional methods, based on adsorption of gases, yield invaluable information about the global features of nanoporous solids, deeper insights pertaining to the local nature of the nanoporosity are best retrieved using ET, as recently exemplified in the work of Yuan et al.[18] Here, slices through the ET reconstruction of SBA-15 mesoporous silica revealed the presence of locally disordered and randomly distributed merged pores (Figure 4b–e). Such local disorder is not detectable in a single 2D TEM image (Figure 4a), which provides only a projection of the structure through hundreds of layers. Moreover, ET proved vital in showing that increases in pore fraction detected by nitrogen sorption for samples subjected to higher temperature hydrothermal treatments were due to increases in the number and volume

fraction of disordered merged pores and not to changes in the sizes of the ordered pores. Similarly, with a hydrothermally treated microporous zeolitic catalyst, it has been shown[19] by ET that this material possesses a hierarchical porosity within single-crystal specimens, and such porosity can be quantified in detail by applying image analysis techniques to the ET reconstructions.[20]

3.3. Nanoparticles with Plasmonic Responses. Solids falling within the size range 1–100 nm are well-known to exhibit chemical properties that are critically dependent upon their precise shape and morphology.[4] Whereas conventional STEM and other high-resolution microscopic techniques that yield 2D images cannot reveal the morphology of such nanoparticles, the ET approach outlined above can.

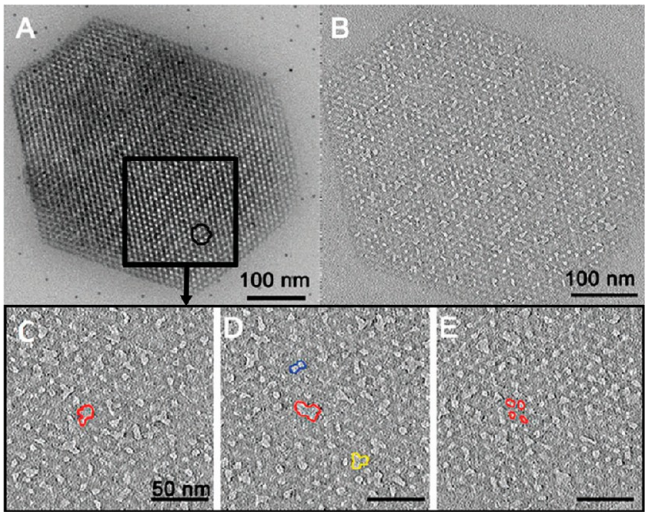

FIGURE 4. (a) BF-TEM image of an ordered mesoporous silica (SBA-15) recorded parallel to the [001] zone axis, showing long-range order. (b) Slice through an ET reconstruction, showing the presence of local disorder caused by randomly distributed merged pores, examples of which are highlighted in color in (c–e), which are slices taken at different heights from the boxed region in panel (a).[18]

A prime example is a recent study[21] linking the plasmonic response of a Au nanoparticle to its true morphology. STEM tomography showed the nanoparticle to have a 3D shape markedly different from the one that would be inferred from a single 2D image (Figure 5a–c). Using the ET reconstruction, the morphology of the nanoparticle was encoded as finite elements and used as input to 3D electrodynamics simulations.[21] By comparing simulations performed using a model based on the true irregular morphology, with those using an idealized shape assumed from a 2D (S)TEM image, dramatic differences in the predicted optical properties were found (Figure 5d).

3.4. Densely-Packed Nanoparticle Systems and Quantitative Analysis. The analysis of agglomerates, mixtures, and composite structures containing densely-packed nanoparticles poses a severe challenge for conventional electron microscopy (TEM or STEM), because image interpretation is hampered by multiple overlapping particles in projection. While 3D tomographic reconstructions can overcome this through slice-by-slice visualization of the tomogram, quantitative analysis of, for example, surface area, volume, crystallography, or porosity requires "segmentation" of the data set, in which each voxel (volume pixel) in the tomogram is assigned to a feature of interest, for instance, a nanoparticle, the vacuum, or the substrate. Such quantification can then be of great value in understanding physical and chemical behavior, illustrated by our first example in this section, in which the 3D morphology of CdSe nanoparticles is key to the performance of certain nanoparticle–polymer blend photovoltaic devices.[22] Figure 6a shows the quantum efficiency as a function of wavelength for thin film photovoltaic devices with different nanoparticle morphology and concentration. STEM-based ET reconstructions confirmed that spherical nanoparticles were distributed homogeneously throughout the polymer matrix and that an increase in their concentration led to

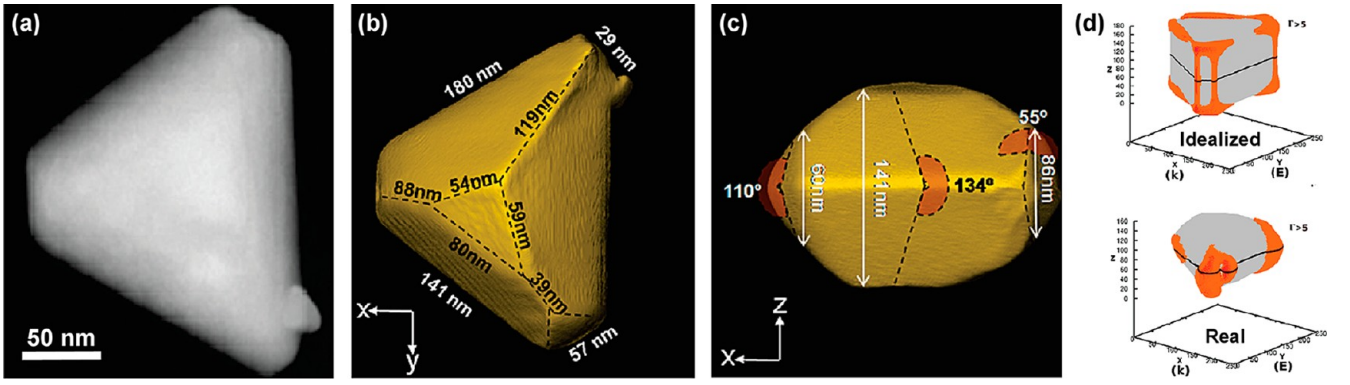

FIGURE 5. (a) HAADF-STEM image of a Au nanoparticle from an ET tilt series. (b,c) Surface-rendered views of the ET reconstructed Au nanoparticle, with dimensions indicated. (d) 3D simulations for the real (using the tomogram) and an idealized (estimated from a single image) nanoparticle, showing regions of high electromagnetic-field enhancement (marked in orange), revealing very different localization.[21]

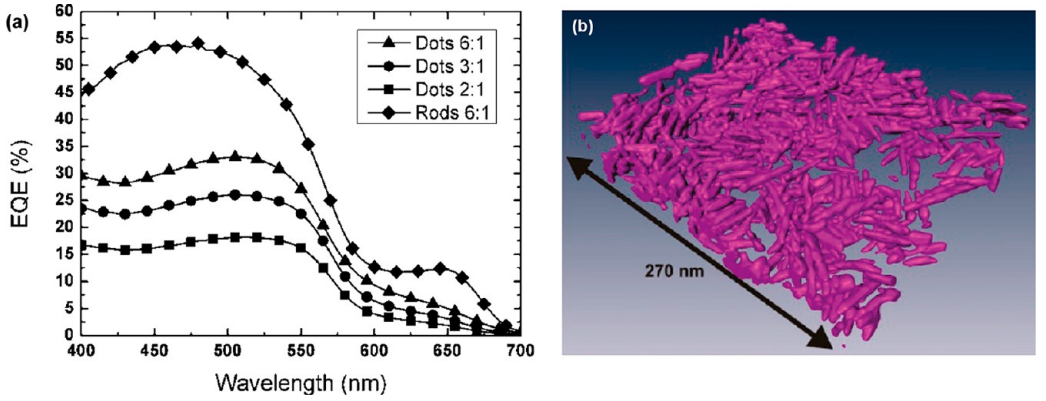

FIGURE 6. (a) Short-circuit external quantum efficiency (EQE) as a function of wavelength for thin film photovoltaic devices with different weight ratios of nanodots or nanorods to polymer. (b) Surface-rendering of an ET reconstruction of the CdSe nanorod network in a nanorod–polymer thin film.[22]

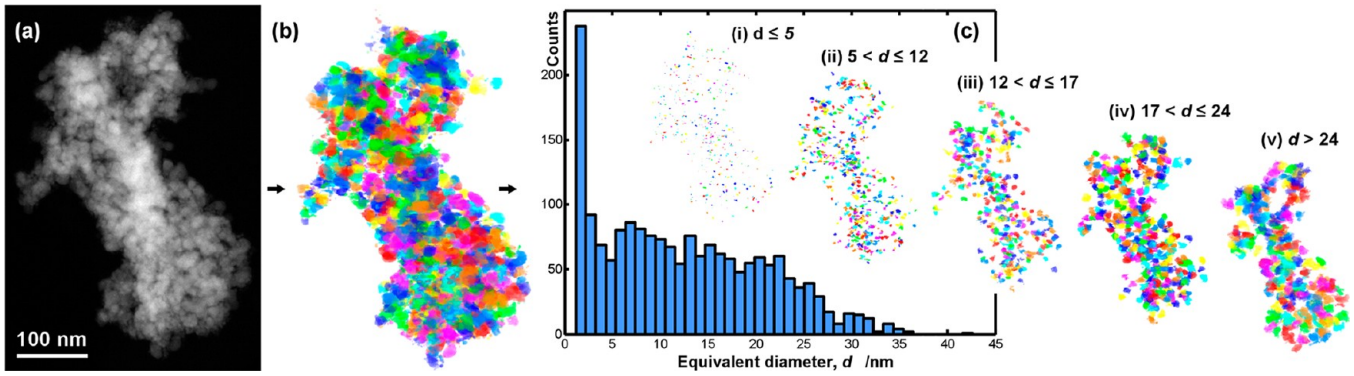

FIGURE 7. (a) HAADF-STEM image of densely-packed $GaPd_2$ nanocrystals from an ET tilt series. (b) 3D voxel-projection visualization of the segmented ET reconstruction, in which each nanocrystal or agglomerate has been given a color that differs from those of its nearest neighbors. (c) Statistical distribution and size filtered tomograms according to the equivalent diameter, *d*, of the nanocrystals and agglomerates.[23]

increased connectivity, and thus to improved charge transport and quantum efficiency. The distribution of nanorods, illustrated in Figure 6b, was also homogeneous but their high aspect ratio and connectivity, seen in the ET reconstructions, led to considerably improved device efficiency.

Most segmentation is undertaken in a manual fashion, which is both time-consuming and prone to error and bias. To process data sets in a fast and routine fashion, automated segmentation methods are being developed based on combinations of image processing tools. We illustrate progress in this area by focusing on the analysis of $GaPd_2$ nanocrystals,[23] ca. 1–30 nm in diameter, recently introduced as novel selective hydrogenation catalysts. Figure 7a shows a HAADF-STEM image of densely-packed $GaPd_2$ nanocrystals. A tilt series of such images yielded a sufficiently high contrast reconstruction to enable a semi-automated segmentation procedure (involving noise reduction, thresholding, and color coding of individual nanocrystals and agglomerates), which revealed with far greater clarity the complex 3D morphology, as shown in Figure 7b. Such a procedure enables a full structural analysis to be undertaken in a more routine and objective way. As an example, Figure 7c shows pictorially, and in histogram form, the size distribution of the $GaPd_2$ nanocrystals and agglomerates.[23] Automation of the segmentation process is a critical step in making ET a more routine analytical tool for the materials chemist and will inevitably be the focus of much attention in the future.

4. Advanced Methods for ET

4.1. Reconstruction Algorithms. The desire for routine quantitative 3D structural information emphasizes the need for reliable, robust reconstruction algorithms to produce high-fidelity 3D tomograms free from artifacts. Inevitably, the limited data sets used in any form of ET, whether they arise from finite angular sampling or a limited tilt range, will lead to imperfect reconstructions. To use such limited data for quantitative 3D analysis requires careful appraisal of how the reconstruction is affected or, better still, the use of new reconstruction algorithms that aim to reduce those artifacts by incorporating known additional (so-called "prior") information about the object to be reconstructed.

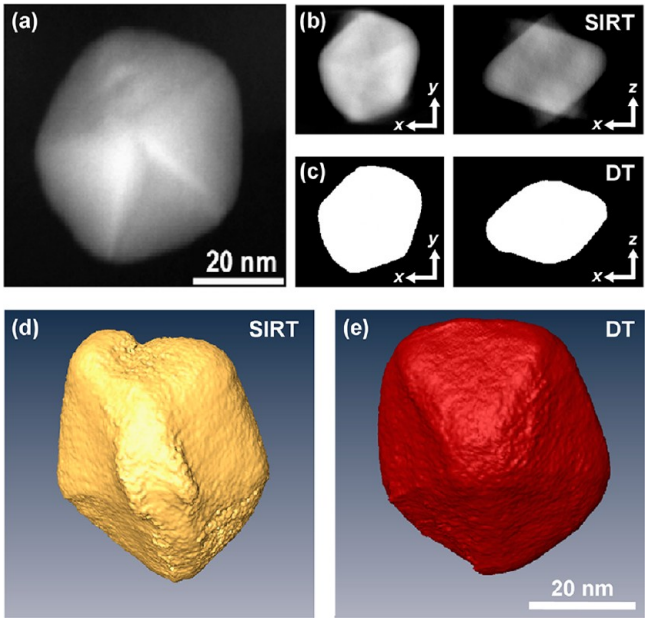

FIGURE 8. (a) HAADF-STEM image of a decahedral Au nanoparticle from a 15 image ET tilt series. (b,c) Orthogonal slices through SIRT and DT 3D reconstructions. (d,e) Surface-rendered views of the reconstructions.[25]

Briefly, we describe two conventional algorithms. The first, weighted back-projection (WBP) compensates, using a linear filter in Fourier space, for the uneven sampling of spatial frequencies brought about by the acquisition of images about a tilt axis. This filter has the effect of enhancing edges and boundaries, ideal for many biological applications where delineation of membrane structures is often key, but is of less value for true quantitative analysis. The second is the simultaneous iterative reconstruction technique (SIRT),[24] which iteratively improves a back-projected reconstruction by minimizing the difference between reprojections of the 3D reconstruction and the original images. This algorithm is the most popular of many possible iterative algebraic reconstruction techniques (ARTs). Now we focus on two new ARTs that allow prior information to be incorporated into the reconstruction process: (i) *discrete tomography* and (ii) *compressed sensing*.

4.1.1. Discrete Tomography. Discrete tomography (DT) reconstruction is an ART that imposes "discreteness" on the object being reconstructed.[7,25] For specimens relevant to materials chemistry, the discrete nature may be either (i) that the object is composed of discrete constituents (e.g., atoms), which may be assumed to lie on a regular 3D grid[26] (see section 4.2 for an elaboration of this) or (ii) that the object is composed of a discrete (typically <5) number of homogeneous phases, meaning in practical terms a discrete number of gray levels in the 3D reconstruction. Such a discrete constraint can be used to great effect, as shown in Figure 8.[25] Here, a multiply twinned (decahedral) nanoparticle has been reconstructed assuming it is composed only of a single species (Au in this case). With this prior knowledge, a high-fidelity reconstruction from only 15 images is possible, alleviating in particular in this example the problem of the missing wedge, as clearly demonstrated by comparison with the equivalent SIRT reconstruction. While this approach is successful, strong constraints are needed based on key assumptions about the sample (for example, the particle contains only Au). So-called "partially discrete" methods that relax these constraints are under development.[27]

4.1.2. Compressed Sensing Electron Tomography (CS-ET). The principles of image compression (e.g., as used for JPEG formats), where images are retrieved from their compressed form without significant information loss, provide an alternative basis for 3D reconstruction from very limited data sets as we have in ET and found often in magnetic resonance imaging[28] and X-ray tomography.[29] The method known as "compressed sensing" (CS) is able to recover a high-fidelity reconstruction from a highly undersampled data set if the object to be reconstructed is "sparse", in this context meaning having relatively few nonzero pixels (or voxels).[8,9] The sparsity may be in the same space as the reconstruction (typically real space) or in some other space linked by a known transform (e.g., in a gradient domain). If the object can be approximated in a sparse way, it is said to be "compressible". To ensure a high-fidelity reconstruction, free from aliasing artifacts, for example, sampling of the object should be performed in a random (or near-random) fashion.[28] A tilt series, as acquired in ET, has been shown to provide a sampling scheme that, although clearly not random, results in aliasing artifacts that are sufficiently "noise-like" that they can be removed by CS. Thus for ET, the CS reconstruction proceeds by finding the sparsest representation of the object to be reconstructed, subject to reprojections of that object best-fitting the original microscope images. Here, the knowledge that the object is in some sense "sparse" provides the extra prior information that improves the reconstruction.

Recently, the authors, in collaboration with the Gladden group in Cambridge (especially D.J. Holland) have shown that CS applied to ET can yield high-fidelity 3D reconstructions from very few images. One example, a CS-ET reconstruction of concave iron oxide nanoparticles,[30] illustrated in Figure 9, demonstrates how, compared with SIRT, CS-ET provides a faithful reconstruction of the octahedral

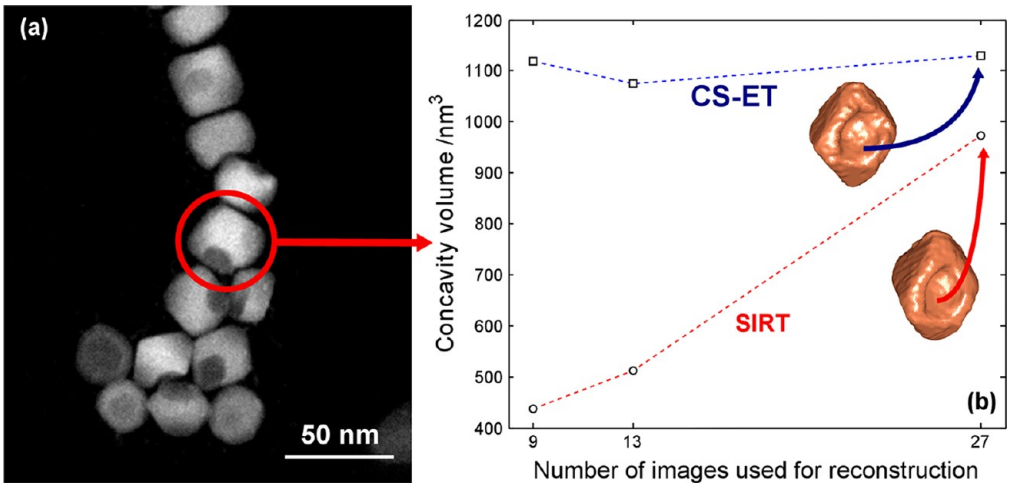

FIGURE 9. (a) HAADF-STEM image of concave iron oxide nanoparticles taken from an ET tilt series. (b) Quantification of the concavity volume of the nanoparticle indicated in panel (a) from CS-ET and SIRT reconstructions using different numbers of images.[30]

morphology and a robust quantitative measurement of the nanoparticle concavity, even from a tilt series composed of only nine images. Knowledge of precise 3D morphology, such as the concavity, is key for application of the particles in drug delivery and photocatalysis.[31]

Compared with DT, CS-ET potentially offers a more flexible approach to how constraints can be applied. For example, for homogeneous objects with sharp boundaries, sparsity may be found in the gradient domain by minimizing the so-called "total variation",[30,32] or for more diffuse objects (e.g., those with compositional gradients), wavelet representations can be used, as they are for JPEG compression in digital photography. Although still in its infancy, we expect CS-ET to be adopted widely in the future. In particular, the ability of CS-ET to yield high-fidelity reconstructions from relatively few images should prove to be of great benefit in the study of beam-sensitive samples or where total acquisition time is limited.

4.2. ET with Atomic Sensitivity. While the use of nanoscale ET in materials chemistry has increased significantly over the past decade, there is still the pressing need to extend the technique to investigate 3D structure at the atomic scale. With the advent of AC optics, atomic resolution in 2D is now commonplace, but extending this to the third dimension is not so straightforward. Here we briefly describe some recent advances.

An estimate of the reconstruction resolution from a conventional tilt series is given by the product of the angular spacing between the images and the size of the object: for a 1 Å 3D resolution, the maximum object that can be reconstructed (using say 100 images) is ~3 nm.[14] Such an approach was undertaken by Bar Sadan et al.[33] using AC-TEM, studying the lattice arrangement in fullerene-like metal oxide nanoparticles. Despite the limited tilt range used (ca. ±30°), a square arrangement of atoms at the nanoparticle apex was revealed, which had been predicted by theory but not seen previously. However, the overall 3D resolution was not sufficient to see the full atomic arrangement in all three dimensions.

By increasing the convergence angle in an AC-STEM, the lateral probe size is kept at or below 1 Å in size, allowing clear imaging of individual atomic columns, but the depth of field, which varies as the inverse square of the convergence angle, can be reduced to just a few nanometers. Depth-sensitive experiments are then possible, in which the beam is focused progressively through the sample thickness, acquiring images sequentially in a fashion akin to confocal microscopy. This has proven to be a powerful method to highlight the position of individual dopant atoms within a matrix,[34,35] but to date has not demonstrated 3D atomic resolution in the true sense. One may speculate whether, with a suitable adjustment of the lens aberrations, it may be possible to sacrifice lateral resolution to improve depth resolution, yielding a more isotropic 3D resolution. True confocal STEM can be achieved by imaging the probe through an aperture in the image plane. However, to retain atomic resolution requires a double aberration-corrected microscope, with correction of the probe-forming lens and the imaging system, to enable an atomic resolution image of the electron beam to be formed in the confocal aperture.[36]

Alternatively, using high-resolution HAADF-STEM images in particular, it may be possible to quantify directly the image intensity and estimate the number of atoms in each atomic column. Such an "atom counting" approach was used to

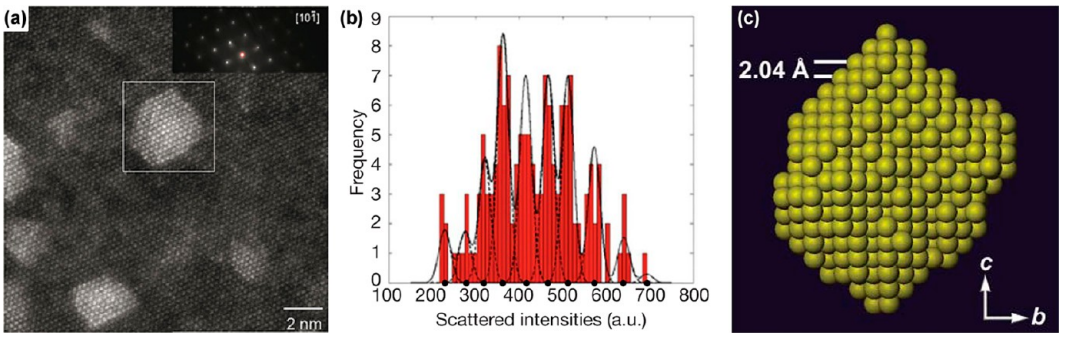

FIGURE 10. (a) HAADF-STEM image of an Ag nanocrystal embedded in an Al matrix. (b) Discrete quantification of the image intensities of the nanocrystal boxed in panel (a). (c) 3D reconstruction of the atomic lattice of the Ag nanocrystal.[26]

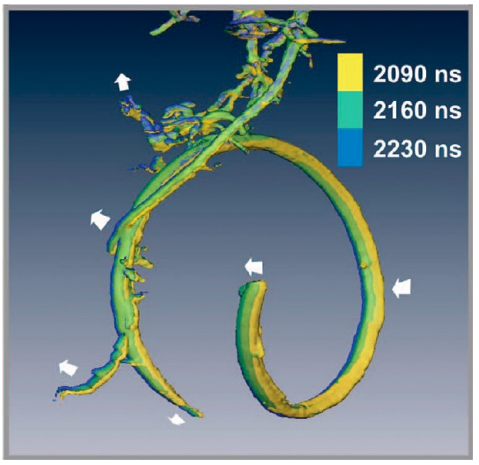

FIGURE 11. Combined ET reconstructions of a carbon nanotube at different instants in time, revealing an oscillatory motion indicated by the white arrows.[10] The field of view is ~1000 nm.

construct 3D atomic pictures of Au nanoclusters from single HAADF images and by comparison with model geometry.[37] More recently van Aert et al.[26] used HAADF-STEM images of an Ag nanocrystal encapsulated within an Al matrix to reconstruct the 3D atomic structure of the nanocrystal (Figure 10). In their approach, the projected intensity of each atomic column was quantified using a best fit statistical method incorporating the discrete constraint (see section 4.1.1) that each column is composed only of a discrete number of atoms (of the same species) and that the 3D lattice is periodic.

While in this case the periodicity constraint is justified, the Ag nanocrystal is embedded within an Al matrix, in general, finite atomic lattices are not necessarily periodic, with atoms at the surface in particular undergoing relaxation or surface reconstruction. This poses a far greater challenge, and different constraints are needed to enable a high-fidelity reconstruction. Moreover, the quantification of atom intensities is only possible while the relationship between atom counts and intensity is monotonic. For thicker samples and heavier atom species, the effects of dynamical diffraction (channeling) become stronger, and image interpretation becomes far more complex.

4.3. Time-Resolved ET. Since many structures or chemical processes are transient in nature, the development of time-resolved ET[10] is of great significance. The essence of the approach developed by Zewail and co-workers[11] is, using stroboscopic methods, to initiate structural changes in the object of interest via laser controlled pulses and then to capture images of the object at subsequent instants, using precisely time-delayed electron pulses, in so-called "pump–probe" experiments. By repetition of this process at different tilt angles, ET reconstructions provide a time-resolved series of tomograms, and in a recent proof-of-principle study,[10] the oscillatory motion of a multiwall carbon nanotube was visualized in 3D (Figure 11). The potential impact of this method to study similar systems is enormous, especially if combined with modern reconstruction algorithms, such as CS-ET, that can greatly reduce the number of images needed in a tilt series.

5. Concluding Remarks

We highlight a few applications that, owing to recent advances, may now become amenable to study by ET. We also speculate on future technique developments that may further enhance the role played by ET in materials chemistry.

5.1. Future Nanochemical Investigations Amenable to ET. 5.1.1. Biomineralization. Our knowledge of biominerals such as $CaCO_3$, bioapatite, and silica has been largely retrieved through the deployment of conventional scanning electron microscopy at comparatively low spatial resolution. However, Pouget et al., in a seminal study,[38] traced the initial stages of template-controlled $CaCO_3$ by cryo-TEM and, in so doing, uncovered the occurrence of nanoscopic prenucleation clusters of the biominerals. It is likely that CS-ET will now open up the feasibility of deeper structural studies of

biomineralization and cognate topics. And in view of the recently disclosed "big bang" approach to ET,[39] which seems best suited to ultrathin specimens of light elements, it may be feasible to explore the early stages of prenucleation of monolayers of proteinaceous material on very thin layers of SiO_2 and $CaCO_3$. It is already known from earlier work in this laboratory and elsewhere on magnetotactic bacteria[4] that ET is an instructive technique for shedding light on the disposition of minute (single) crystals of Fe_3O_4 surrounded by its biological shroud.

5.1.2. Nanoparticle Inorganic Oxides as Substitute Enzymes. It is remarkable that nanoparticles of magnetic materials, such as magnetite (Fe_3O_4) and its congener Co_3O_4, in the size range of 30 to 300 nm can exhibit intrinsic peroxidase-like activity.[40,41] Much work now needs to be done to identify the precise crystal facets in these nanoparticles where the greatest enzymatic activity is exhibited. It may also transpire that microspheres of Co_3O_4 will exhibit high enzyme-like performance, just as they do in their role as ethanol sensors.[42]

5.1.3. Dielectric and Energy Storage Properties of High-Permittivity Metal Oxide Nanocomposites. It is recognized that materials having high dielectric permittivity, high breakdown strength, low loss, and fast response will be essential for future electrical and electronic applications. A full discussion of the materials chemistry aspects of such applications has been given recently by Lanagan, Ratner, Marks, and coworkers.[43] Here, cores of $BaTiO_3$ or ZrO_2 and thin (variable) shells of Al_2O_3 are the key components. The nature of such encapsulated materials could be further elucidated by the application of ET in its various modes, as outlined in this Account. In particular, the precise distribution and interfacial properties of the polyolefin that surrounds the Al_2O_3-encapsulated nanoparticles could be retrieved at high spatial resolution.

5.2. Future Advances in ET Techniques. The ability to incorporate prior knowledge into reconstruction algorithms has enabled high-fidelity reconstructions to be made from very limited data sets. Further work is needed to ensure that the techniques are reliable and provide trustworthy, truly quantitative results for every data set. But once a robust methodology is in place, genuine "3D nanometrology" (measurement with statistically meaningful errors) may be realized. With both DT and CS-ET approaches providing high-contrast reconstructions, fully automated segmentation routines may be possible in the near future. The advent of aberration correction has led to routine sub-Ångström atomic resolution 2D imaging, but 3D atomic resolution in the most general case is still elusive. Physical constraints, regarding, for example, periodicity and atomicity, can be combined with knowledge of the reconstruction (e.g., positivity, sparsity) to improve both the reconstruction fidelity and resolution, and new, more flexible, algorithmic approaches need to be developed further. Modern (S)TEMs not only act as remarkably efficient microscopes yielding structural information at the highest resolution but also, with the availability of highly coherent electron sources, monochromators, and sensitive spectrometers, yield spectroscopic information that provides a unique insight into the 3D chemical nature of many materials. Time-resolved stroboscopic imaging adds another dimension to what may be achieved with a (S)TEM and, coupled with ET and novel reconstruction algorithms, should provide a new understanding of many time-dependent physicochemical phenomena with sub-nanometer 3D resolution. Lastly, the availability of environmental cells and specialized specimen holders could allow tomographic analysis of materials when subject to high (or low) temperatures, a reactive gas, mechanical stress, or other stimuli. Combining such in situ capabilities[44] with 3D imaging (possibly time-resolved) would provide an extraordinary ensemble of tools that would inevitably lead to a deeper understanding in many fields of materials chemistry.

We thank D.J. Holland and co-workers for their invaluable role in the development of CS-ET. P.A.M. acknowledges financial support from the ERC, Reference 291522 3DIMAGE.

BIOGRAPHICAL INFORMATION

Rowan Leary obtained a 1st class MEng/BEng from the University of Leeds in 2010. He is currently a Ph.D. student under the supervision of Professor Paul Midgley.

Paul Midgley is Professor of Materials Science at the Department of Materials Science and Metallurgy, University of Cambridge. He has been the pioneer of many novel electron microscopical techniques and in 2007 was awarded the Ernst Ruska Prize.

John Meurig Thomas is currently honorary Professor of solid-state chemistry at Cambridge and is renowned for his work in catalysis and solid-state, materials, and surface chemistry.

FOOTNOTES

*Corresponding authors. E-mail, rkl26@cam.ac.uk; tel, +44(0)1223334597. E-mail, pam33@cam.ac.uk; tel, +44(0)1223334561; fax, +44(0)1223334567. E-mail, jmt2@cam.ac.uk; tel, +44(0)1223334300; fax, +44(0)1223334567.
The authors declare no competing financial interest.

REFERENCES

1 Midgley, P. A.; Weyland, M.; Thomas, J. M.; Johnson, B. F. G. Z-Contrast Tomography: A Technique in Three-Dimensional Nanostructural Analysis Based on Rutherford Scattering. *Chem. Commun.* **2001**, 907–908.

2 Thomas, J. M.; Johnson, B. F. G.; Raja, R.; Sankar, G.; Midgley, P. A. High-Performance Nanocatalysts for Single-Step Hydrogenations. *Acc. Chem. Res.* **2003**, *36*, 20–30.

3 Friedrich, H.; de Jongh, P. E.; Verkleij, A. J.; de Jong, K. P. Electron Tomography for Heterogeneous Catalysts and Related Nanostructured Materials. *Chem. Rev.* **2009**, *109*, 1613–1629.

4 Midgley, P. A.; Ward, E. P. W.; Hungria, A. B.; Thomas, J. M. Nanotomography in the Chemical, Biological and Materials Sciences. *Chem. Soc. Rev.* **2007**, *36*, 1477–1494.

5 Thomas, J. M.; Midgley, P. A. The Modern Electron Microscope: A Cornucopia of Chemico-physical Insights. *Chem. Phys.* **2011**, *385*, 1–10.

6 Thomas, J. M.; Midgley, P. A.; Yates, T. J. V.; Barnard, J. S.; Raja, R.; Arslan, I.; Weyland, M. The Chemical Application of High-Resolution Electron Tomography: Bright Field or Dark Field? *Angew. Chem., Int. Ed.* **2004**, *43*, 6745–6747.

7 Herman, G. T.; Kuba, A. *Advances in Discrete Tomography and Its Applications*; Birkhauser: Boston, MA, 2007.

8 Candès, E. J.; Romberg, J.; Tao, T. Robust Uncertainty Principles: Exact Signal Reconstruction from Highly Incomplete Frequency Information. *IEEE Trans. Inf. Theory* **2006**, *52*, 489–509.

9 Donoho, D. L. Compressed Sensing. *IEEE Trans. Inf. Theory* **2006**, *52*, 1289–1306.

10 Kwon, O.-H.; Zewail, A. H. 4D Electron Tomography. *Science* **2010**, *328*, 1668–1673.

11 Zewail, A. H.; Thomas, J. M. *4D Electron Microscopy: Imaging in Space and Time*; Imperial College Press: Hackensack, NJ, 2010.

12 Midgley, P. A.; Thomas, J. M.; Laffont, L.; Weyland, M.; Raja, R.; Johnson, B. F. G.; Khimyak, T. High-Resolution Scanning Transmission Electron Tomography and Elemental Analysis of Zeptogram Quantities of Heterogeneous Catalyst. *J. Phys. Chem. B* **2004**, *108*, 4590–4592.

13 Frank, J. *Electron Tomography: Methods for Three-Dimensional Visualization of Structures in the Cell*; Springer: New York; London, 2006.

14 Crowther, R. A.; DeRosier, D. J.; Klug, A. The Reconstruction of a Three-Dimensional Structure from Projections and its Application to Electron Microscopy. *Proc. R. Soc. London, Ser. A* **1970**, *317*, 319–340.

15 Ward, E. P. W.; Yates, T. J. V.; Fernández, J.-J.; Vaughan, D. E. W.; Midgley, P. A. Three-Dimensional Nanoparticle Distribution and Local Curvature of Heterogeneous Catalysts Revealed by Electron Tomography. *J. Phys. Chem. C* **2007**, *111*, 11501–11505.

16 Hernández-Garrido, J. C.; Yoshida, K.; Gai, P. L.; Boyes, E. D.; Christensen, C. H.; Midgley, P. A. The Location of Gold Nanoparticles on Titania: A Study by High Resolution Aberration-Corrected Electron Microscopy and 3D Electron Tomography. *Catal. Today* **2011**, *160*, 165–169.

17 Yu, Y.; Xin, H. L.; Hovden, R.; Wang, D.; Rus, E.; Mundy, J.; Muller, D. A.; Abruña, H. D. Three-Dimensional Tracking and Visualization of Hundreds of Pt-Co Fuel Cell Nanocatalysts During Electrochemical Aging. *Nano Lett.* **2011,** DOI: 10.1021/nl203920s.

18 Yuan, P.; Tan, L.; Pan, D.; Guo, Y.; Zhou, L.; Yang, J.; Zou, J.; Yu, C. A Systematic Study of Long-Range Ordered 3D-SBA-15 Materials by Electron Tomography. *New J. Chem.* **2011**, *35*, 2456–2461.

19 de Jong, K. P.; Zečević, J.; Friedrich, H.; de Jongh, P. E.; Bulut, M.; van Donk, S.; Kenmogne, R.; Finiels, A.; Hulea, V.; Fajula, F. Zeolite Y Crystals with Trimodal Porosity as Ideal Hydrocracking Catalysts. *Angew. Chem.* **2010**, *122*, 10272–10276.

20 Zečević, J.; Gommes, C. J.; Friedrich, H.; de Jongh, P. E.; de Jong, K. P. Mesoporosity of Zeolite Y: Quantitative Three-Dimensional Study by Image Analysis of Electron Tomograms. *Angew. Chem., Int. Ed.* **2012**, *51*, 4213–4217.

21 Perassi, E. M.; Hernandez-Garrido, J. C.; Moreno, M. S.; Encina, E. R.; Coronado, E. A.; Midgley, P. A. Using Highly Accurate 3D Nanometrology to Model the Optical Properties of Highly Irregular Nanoparticles: A Powerful Tool for Rational Design of Plasmonic Devices. *Nano Lett.* **2010**, *10*, 2097–2104.

22 Hindson, J. C.; Saghi, Z.; Hernandez-Garrido, J.-C.; Midgley, P. A.; Greenham, N. C. Morphological Study of Nanoparticle-Polymer Solar Cells Using High-Angle Annular Dark-Field Electron Tomography. *Nano Lett.* **2011**, *11*, 904–909.

23 Leary, R.; Saghi, Z.; Armbrüster, M.; Wowsnick, G.; Schlögl, R.; Thomas, J. M.; Midgley, P. A. Quantitative High-Angle Annular Dark-Field Scanning Transmission Electron Microscope (HAADF-STEM) Tomography and High-Resolution Electron Microscopy of Unsupported Intermetallic $GaPd_2$ Catalysts. *J. Phys. Chem. C* **2012**, *116*, 13343–13352.

24 Gilbert, P. Iterative Methods for the Three-Dimensional Reconstruction of an Object from Projections. *J. Theor. Biol.* **1972**, *36*, 105–117.

25 Batenburg, K. J.; Bals, S.; Sijbers, J.; Kübel, C.; Midgley, P. A.; Hernandez, J. C.; Kaiser, U.; Encina, E. R.; Coronado, E. A.; Van Tendeloo, G. 3D Imaging of Nanomaterials by Discrete Tomography. *Ultramicroscopy* **2009**, *109*, 730–740.

26 Van Aert, S.; Batenburg, K. J.; Rossell, M. D.; Erni, R.; Van Tendeloo, G. Three-Dimensional Atomic Imaging of Crystalline Nanoparticles. *Nature* **2011**, *470*, 374–377.

27 Roelandts, T.; Batenburg, K. J.; Biermans, E.; Kübel, C.; Bals, S.; Sijbers, J. Accurate Segmentation of Dense Nanoparticles by Partially Discrete Electron Tomography. *Ultramicroscopy* **2012**, *114*, 96–105.

28 Lustig, M.; Donoho, D.; Pauly, J. M. Sparse MRI: The Application of Compressed Sensing for Rapid MR Imaging. *Magn. Reson. Med.* **2007**, *58*, 1182–1195.

29 Sidky, E. Y.; Kao, C.-M.; Pan, X. Accurate Image Reconstruction from Few-Views and Limited-Angle Data in Divergent-Beam CT. *J. X-Ray Sci. Technol.* **2006**, *14*, 119–139.

30 Saghi, Z.; Holland, D. J.; Leary, R.; Falqui, A.; Bertoni, G.; Sederman, A. J.; Gladden, L. F.; Midgley, P. A. Three-Dimensional Morphology of Iron Oxide Nanoparticles with Reactive Concave Surfaces. A Compressed Sensing-Electron Tomography (CS-ET) Approach. *Nano Lett.* **2011**, *11*, 4666–4673.

31 George, C.; Dorfs, D.; Bertoni, G.; Falqui, A.; Genovese, A.; Pellegrino, T.; Roig, A.; Quarta, A.; Comparelli, R.; Curri, M. L.; Cingolani, R.; Manna, L. A Cast-Mold Approach to Iron Oxide and Pt/Iron Oxide Nanocontainers and Nanoparticles with a Reactive Concave Surface. *J. Am. Chem. Soc.* **2011**, *133*, 2205–2217.

32 Goris, B.; Van den Broek, W.; Batenburg, K. J.; Heidari Mezerji, H.; Bals, S. Electron Tomography Based on a Total Variation Minimization Reconstruction Technique. *Ultramicroscopy* **2012**, *113*, 120–130.

33 Bar Sadan, M.; Houben, L.; Wolf, S. G.; Enyashin, A.; Seifert, G.; Tenne, R.; Urban, K. Toward Atomic-Scale Bright-Field Electron Tomography for the Study of Fullerene-Like Nanostructures. *Nano Lett.* **2008**, *8*, 891–896.

34 van Benthem, K.; Lupini, A. R.; Kim, M.; Baik, H. S.; Doh, S.; Lee, J.-H.; Oxley, M. P.; Findlay, S. D.; Allen, L. J.; Luck, J. T.; Pennycook, S. J. Three-Dimensional Imaging of Individual Hafnium Atoms Inside a Semiconductor Device. *Appl. Phys. Lett.* **2005**, *87*, No. 034104.

35 Allen, J. E.; Hemesath, E. R.; Perea, D. E.; Lensch-Falk, J. L.; LiZ., Y; Yin, F.; Gass, M. H.; Wang, P.; Bleloch, A. L.; Palmer, R. E.; Lauhon, L. J. High-Resolution Detection of Au Catalyst Atoms in Si Nanowires. *Nat. Nanotechnol.* **2008**, *3*, 168–173.

36 Nellist, P. D.; Behan, G.; Kirkland, A. I.; Hetherington, C. J. D. Confocal Operation of a Transmission Electron Microscope with Two Aberration Correctors. *Appl. Phys. Lett.* **2006**, *89*, No. 124105.

37 Li, Z. Y.; Young, N. P.; Di Vece, M.; Palomba, S.; Palmer, R. E.; Bleloch, A. L.; Curley, B. C.; Johnston, R. L.; Jiang, J.; Yuan, J. Three-Dimensional Atomic-Scale Structure of Size-Selected Gold Nanoclusters. *Nature* **2008**, *451*, 46–48.

38 Pouget, E. M.; Bomans, P. H. H.; Goos, J. A. C. M.; Frederik, P. M.; de With, G.; Sommerdijk, N. A. J. M. The Initial Stages of Template-Controlled $CaCO_3$ Formation Revealed by Cryo-TEM. *Science* **2009**, *323*, 1455–1458.

39 Van Dyck, D.; Chen, F.-R. 'Big Bang' Tomography As a New Route to Atomic-Resolution Electron Tomography. *Nature* **2012**, *486*, 243–246.

40 Mu, J.; Wang, Y.; Zhao, M.; Zhang, L. Intrinsic Peroxidase-like Activity and Catalase-like Activity of Co_3O_4 Nanoparticles. *Chem. Commun.* **2012**, *48*, 2540–2542.

41 Gao, L.; Zhuang, J.; Nie, L.; Zhang, J.; Zhang, Y.; Gu, N.; Wang, T.; Feng, J.; Yang, D.; Perrett, S.; Yan, X. Intrinsic Peroxidase-like Activity of Ferromagnetic Nanoparticles. *Nat. Nanotechnol.* **2007**, *2*, 577–583.

42 Sun, C.; Rajasekhara, S.; Chen, Y.; Goodenough, J. B. Facile synthesis of monodisperse porous Co_3O_4 microspheres with superior ethanol sensing properties. *Chem. Commun.* **2011**, *47*, 12852–12854.

43 Li, Z.; Fredin, L. A.; Tewari, P.; DiBenedetto, S. A.; Lanagan, M. T.; Ratner, M. A.; Marks, T. J. In Situ Catalytic Encapsulation of Core-Shell Nanoparticles Having Variable Shell Thickness: Dielectric and Energy Storage Properties of High-Permittivity Metal Oxide Nanocomposites. *Chem. Mater.* **2010**, *22*, 5154–5164.

44 Gai, P. L.; Sharma, R.; Ross, F. M. Environmental (S)TEM Studies of Gas−Liquid−Solid Interactions under Reaction Conditions. *MRS Bull.* **2008**, *33*, 107–114.